

Analysis of spin density wave conductivity spectra of iron pnictides in the framework of density functional theory

Johannes Ferber,* Yu-Zhong Zhang, Harald O. Jeschke, and Roser Valentí
*Institut für Theoretische Physik, Goethe-Universität Frankfurt,
 Max-von-Laue-Strasse 1, 60438 Frankfurt/Main, Germany*
 (Dated: June 4, 2018)

The optical conductivity of LaFeAsO, BaFe₂As₂, SrFe₂As₂, and EuFe₂As₂ in the spin-density wave (SDW) state is investigated within density functional theory (DFT) in the framework of spin-polarized generalized gradient approximation (GGA) and GGA+U. We find a strong dependence of the optical features on the Fe magnetic moments. In order to recover the small Fe magnetic moments observed experimentally, GGA+ U_{eff} with a suitable choice of negative on-site interaction $U_{\text{eff}} = U - J$ was considered. Such an approach may be justified in terms of an overscreening which induces a relatively small U compared to the Hund's rule coupling J , as well as a strong Holstein-like electron-phonon interaction. Moreover, reminiscent of the fact that GGA+ U_{eff} with a positive U_{eff} is a simple approximation for reproducing a gap with correct amplitude in correlated insulators, a negative U_{eff} can also be understood as a way to suppress magnetism and mimic the effects of quantum fluctuations ignored in DFT calculations. With these considerations, the resulting optical spectra reproduce the SDW gap and a number of experimentally observed features related to the antiferromagnetic order. We find electronic contributions to excitations that so far have been attributed to purely phononic modes. Also, an orbital resolved analysis of the optical conductivity reveals significant contributions from all Fe $3d$ orbitals. Finally, we observe that there is an important renormalization of kinetic energy in these SDW metals, implying that the effects of correlations cannot be neglected.

PACS numbers: 74.70.Xa, 71.15.Mb, 74.25.Gz, 74.25.Jb

I. INTRODUCTION

In several families of the iron pnictides, high temperature superconductivity (SC) emerges in close proximity of an antiferromagnetic (AF) ground state with stripe-type order.¹ The AF transition is induced by a spin-density wave (SDW) instability below a critical temperature T_{SDW} , which is either preceded or coincidental with a structural transition from a tetragonal phase to an orthorhombic phase.² Upon doping³ or application of pressure⁴, the AF order is suppressed and superconductivity emerges. Like lattice vibrations, AF fluctuations are capable of producing an attractive interaction necessary for the creation of Cooper pairs. It is therefore widely believed that the AF fluctuations drive the superconducting instability in these systems. As for the nature of the AF state, the iron pnictides show signatures of both electron itinerancy and local magnetism. Some experimental^{5–11} and theoretical works based on density functional theory (DFT)^{12–18} and dynamical mean-field theory (DMFT)¹⁹ as well as a combination of these two methods^{20,21} favor an itinerant scenario with rather moderate correlation strength, as reflected by the metallic nature of the compounds. On the other hand, other authors point out the effects of strong correlations,^{22–27} like the renormalization of the kinetic energy of the electrons.²⁸

Many features of the electronic structure of the iron pnictides are directly reflected in their optical properties: the low-frequency region of the conductivity spectrum is governed by the itinerant carrier contribution and directly shows the effect of correlations in the area under

the Drude region which is proportional to the electron's kinetic energy; the infrared regime above the Drude peak is dominated by gap features induced by either the SDW gap or the superconducting gap; finally, the visible part of the spectrum reflects the band structure in the normal state. Consequently, a number of experimental studies have been performed on the optical properties of the iron pnictides, in the normal state, the SDW state, as well as in the SC state.^{5,11,29–33,58} The SDW state is characterized by (i) the appearance of a peak in the optical conductivity at the SDW gap frequency, (ii) an anisotropic dc response and (iii) an almost isotropic response in the infrared and optical region of the spectrum. On the other hand, while several theoretical works based on local density approximation (LDA)²⁸ and LDA+DMFT^{24,34} have been done on the paramagnetic phase, there is still a lack of DFT calculations for the optical conductivity in the SDW state.

In this work we report optical studies in the framework of density functional theory on four iron pnictides in the SDW state, namely the 1111 compound LaFeAsO, and the 122 compounds $A\text{Fe}_2\text{As}_2$ ($A\text{E}=\text{Ba},\text{Sr},\text{Eu}$). This provides an insight into the microscopic origin of the optical features in the SDW state and allows for an assessment of DFT regarding its applicability to the iron pnictides.

II. COMPUTATIONAL DETAILS

We performed electronic structure calculations with the full potential linearized augmented plane wave

(FLAPW) method as implemented in WIEN2K.³⁵ The self-consistency cycle employed 2048 k points in the full Brillouin zone (FBZ) using the generalized gradient approximation (GGA) in the Perdew-Burke-Ernzerhof variant for the exchange correlation potential;³⁶ the optical properties were evaluated with 16384 k points in the FBZ, the number of k points in the irreducible Brillouin zone depends on the symmetries of the respective material. Experimental lattice parameters and atomic positions were used, from Refs. 37–40 for LaFeAsO, BaFe₂As₂, SrFe₂As₂, and EuFe₂As₂, respectively. All calculations were performed in the scalar relativistic approximation. For the optical properties, the `optics`⁴¹ code package in WIEN2K was modified to allow for an orbital character resolved analysis.

We are working in the framework of 'GGA+U' where 'U' ($\equiv U_{\text{eff}} = U - J$) describes the competition between the (spherically averaged) on-site Coulomb interaction U and the (spherically averaged) on-site exchange coupling J (within the Fe $3d$ subshell for the iron pnictides). In this context, the atomic limit double counting correction according to Refs. 42 and 54 was applied. With this double counting correction, the expression for the correction to the GGA functional for the orbital m reads

$$\frac{U - J}{2} \sum_{\sigma} n_{m\sigma}(1 - n_{m\sigma}), \quad (1)$$

where $n_{m\sigma}$ is the spin-projected occupation in orbital m .

In order to allow for the stripe-type AF order, we consider a doubled ($\sqrt{2} \times \sqrt{2} \times 1$) unit cell with AF order along the a axis of the supercell and ferromagnetic (FM) arrangement along the b axis (*i.e.* the supercell is rotated 45° with respect to the original unit cell), as observed experimentally. In the following, the orbital characters and dielectric tensor components are labelled with respect to the coordinate system of this supercell. Spin-polarized calculations with AF order are labelled with 'GGA(AF)' ('GGA+U(AF)', respectively).

The linear optical response of the electronic system⁵⁹ is calculated in the random phase approximation (RPA), with the Kohn-Sham orbitals mimicking the bare electronic states of the electron-hole excitations in the RPA formalism. In this framework, the complex-valued dielectric function ϵ is calculated as

$$\epsilon(\omega) = 1 - \lim_{q \rightarrow 0} \frac{4\pi e^2}{\Omega_c |\mathbf{q}|^2} \sum_{n, n', \mathbf{k}} \frac{f_0(E_{n', \mathbf{k} + \mathbf{q}}) - f_0(E_{n, \mathbf{k}})}{E_{n', \mathbf{k} + \mathbf{q}} - E_{n, \mathbf{k}} - \hbar\omega} \times |M_{n, n'}(\mathbf{k}, \mathbf{q})|^2, \quad (2)$$

where Ω_c is the volume of the unit cell, \mathbf{q} the wavevector of the incoming light, f_0 the Fermi distribution, and $\{n, \mathbf{k}\}$ labels the Kohn-Sham (KS) orbital in band n with crystal momentum \mathbf{k} . The transition matrix element is given by $M_{n, n'}(\mathbf{k}, \mathbf{q}) = \langle n, \mathbf{k} | e^{-i\mathbf{q}\mathbf{r}} | n', \mathbf{k} + \mathbf{q} \rangle$. As expressed by $\lim_{q \rightarrow 0}$, only direct transitions $\mathbf{k}_f = \mathbf{k}_i$ are considered here since even for high energies, the wavelength of the light is large compared to the lattice dimensions. In this limit, perturbation theory for $\mathbf{k} \cdot \mathbf{p}$ can

be applied (\mathbf{p} being the momentum operator) in order to obtain expressions for $|n, \mathbf{k} + \mathbf{q}\rangle$ and $E_{n, \mathbf{k} + \mathbf{q}}$ in terms of $|n, \mathbf{k}\rangle$ and $E_{n, \mathbf{k}}$ within the dipole approximation. This yields for the dielectric tensor⁴¹

$$\epsilon_{ij}(\omega) = 1 + \frac{4\pi\hbar^2 e^2}{\Omega_c m^2 \omega^2} \sum_{n, \mathbf{k}} \left(\frac{\partial f_0}{\partial E} \right)_{E_F} p_{i; n, n, \mathbf{k}} p_{j; n, n, \mathbf{k}} - \frac{4\pi\hbar^2 e^2}{\Omega_c m^2} \sum_{\mathbf{k}} \sum_{v, c} \frac{p_{i; c, v, \mathbf{k}} p_{j; c, v, \mathbf{k}}}{(E_{c, \mathbf{k}} - E_{v, \mathbf{k}} - \hbar\omega)(E_{c, \mathbf{k}} - E_{v, \mathbf{k}})^2}, \quad (3)$$

where the second and third term describe the intraband and interband contributions, respectively. Since $T = 0$ is considered, the intraband contribution is restricted to states at the Fermi energy E_F , whereas the band indices $v(c)$ run over all occupied (empty) states. p_i is the matrix element of the momentum operator along the electric field polarization of the incoming light, $p_{i; n, n', \mathbf{k}} = \langle n, \mathbf{k} | p_i | n', \mathbf{k} \rangle$. Spin-orbit coupling is not taken into account in our calculations, and therefore all off-diagonal elements $i \neq j$ vanish due to the orthorhombic symmetry of the crystals.

Turning the sum in Eq. (3) into an integral over the first Brillouin zone and using the Dirac representation $\frac{1}{x \pm i\eta} = \mathcal{P} \frac{1}{x} \mp i\pi\delta(x)$, the imaginary part of the interband contributions to the dielectric tensor components can be expressed as

$$\text{Im } \epsilon_{ii}^{\text{inter}}(\omega) = \frac{\hbar^2 e^2}{\pi m^2 \omega^2} \sum_{v, c} \int_{\mathbf{k}} |p_{i; c, v, \mathbf{k}}|^2 \delta(E_{c, \mathbf{k}} - E_{v, \mathbf{k}} - \hbar\omega). \quad (4)$$

In this work, we focus on the analysis of the real part of the optical conductivity,

$$\text{Re } \sigma_{ij}(\omega) = \frac{\omega}{4\pi} \text{Im } \epsilon_{ij}(\omega). \quad (5)$$

For metals, the intraband contribution has the well-known Drude shape

$$\sigma_D = \frac{\Gamma \omega_p^2}{4\pi(\omega^2 + \Gamma^2)}, \quad (6)$$

where the plasma frequency ω_p determines the spectral weight of the Drude peak via $\int_0^\infty d\omega \sigma_D(\omega) = \frac{\omega_p}{8}$, whereas its width is given by the carrier scattering rate $\Gamma = 1/\tau$ with the lifetime τ .

The presence of the Drude peak depends on the metallicity of the material under consideration and in general needs to be confirmed by an explicit calculation of the intraband transitions. However, as only direct transitions are considered here, the intraband part of Eq. (3) is singular at $\omega = 0$ and vanishes at finite frequencies, both for the dielectric function as well as for the conductivity. Instead, the squared plasma frequency for band n and spin σ is defined as

$$\omega_p^2(n, \sigma) = \frac{\hbar^2 e^2}{\pi m^2} \int_{\mathbf{k}} |\langle n, \mathbf{k}, \sigma | p | n, \mathbf{k}, \sigma \rangle|^2 \delta(E_{n, \mathbf{k}, \sigma} - E_F) \quad (7)$$

with the total squared plasma frequency $\omega_p^2 = \sum_{n,\sigma} \omega_p^2(n,\sigma)$, and the Drude peak is considered as an approximation to the intraband conductivity, *i.e.* we consider only one overall Drude peak, despite the possibility of two or more Drude peaks due to multiple bands crossing the Fermi surface. For the iron pnictides, this is justified as they show metallic behaviour also below the SDW transition. Consequently, only the carrier scattering rate is left as free parameter which cannot be determined within a DFT approach. For our purposes, Γ is chosen close to experimental values⁵ in the SDW state. Given these considerations, all relevant information about the Drude peaks is contained in the plasma frequency ω_p .

III. RESULTS

A. Density of States

Preliminary to the analysis of the optical properties of the iron pnictides, we first start with the discussion of the density of states (DOS) since the dielectric function is essentially the joint density of states (jDOS) weighted with the transition matrix element (see Eq. (4)). In particular, we find that the antiferromagnetic order and the magnitude of the magnetic moments crucially affect the optical properties which is reflected by the (partial) opening of a gap in the DOS.

For the iron pnictides, DFT calculations are known to strongly overestimate the magnetic moments on the Fe atoms in the SDW state ($\approx 2.0\mu_B$ with GGA(AF) compared to $0.4\mu_B$ ⁴³– $0.6\mu_B$ ⁴⁴ for LaFeAsO). As will be discussed in the following, this results in a too large SDW gap which in turn shifts the SDW features in the optical properties to erroneously high energies. In order to reproduce correctly the SDW gap, we employ GGA+U with U_{eff} negative^{7,45} to suppress the overestimated magnetic moment from GGA(AF). On the one hand, the negative U_{eff} can be viewed as a result of an overscreening of the on-site Coulomb interaction which leads to a smaller value of U compared to the on-site exchange interaction J or a strong Holstein-like electron-phonon coupling which gives a frequency-dependent negative contribution to the on-site Coulomb interaction. On the other hand, similar to the application of positive U at the mean-field level in GGA+U calculations to reproduce the correlated gap in Mott insulators, the negative U_{eff} can be understood as a simple way to suppress the tendency to magnetism within the mean-field approximation and mimic the effect of quantum fluctuations ignored in DFT. This can be read off from the correction to the GGA functional in Eq. (1) which energetically favors $n_{m\sigma} = 1/2$ at negative U_{eff} , *i.e.* the paramagnetic case, and conversely penalizes (spin-projected) integer occupations, *i.e.* the fully polarized states. Note that the exact form of the GGA+U functional and thus the preference of low-spin or high-spin states depends on the double counting correction.⁵³

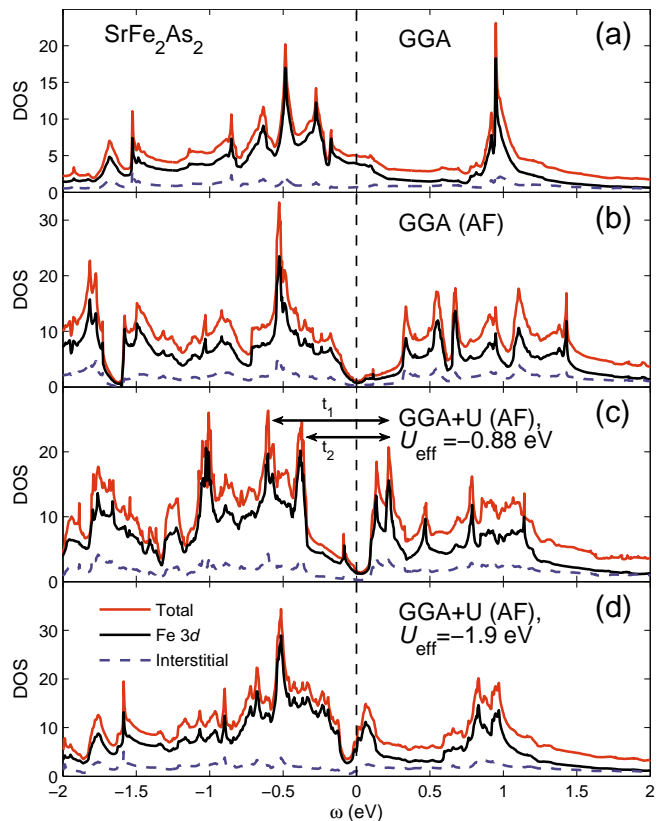


FIG. 1. (Color online) DOS of SrFe_2As_2 for different values of U_{eff} . $\omega = 0$ corresponds to the Fermi energy. As is well known, the Fe $3d$ subshell dominates the DOS around the Fermi energy. The contributions from Sr and As, and the other Fe orbitals are small. The magnetic moments from top to bottom are $m = 0$, $m = 1.98 \mu_B$, $m = 1.30 \mu_B$, and $m = 0.43 \mu_B$, respectively. See text for a discussion of the transitions labelled by t_1 and t_2 .

A comparison of the role of U and J with their model counterparts is therefore not generally valid but needs to take into account the double counting correction under consideration. Also, the magnetic moment needs to be further reduced below its experimental value due to the RPA employed in our calculations of optical conductivities, as discussed later. Therefore, the negative U_{eff} used in this paper is not comparable to realistic values of U and J for these systems due to the approximations we employed here.

Fig. 1 shows the evolution of the density of states for different values of U_{eff} in SrFe_2As_2 . Compared to the non-spin-polarized GGA DOS, a suppression of the DOS around E_F is clearly visible in the antiferromagnetic calculations. For the parameter regimes shown in Fig. 1, only partial opening of the gap is observed as some DOS persists around E_F ; full opening of the gap occurs at positive values of U_{eff} , *i.e.* for sufficiently strong Hubbard U . In contrast, for pronounced negative U_{eff} the magnetic moment is reduced and the SDW gap narrows accordingly. For $U_{\text{eff}} = -1.9 \text{ eV}$ and $m = 0.43 \mu_B$, the energy

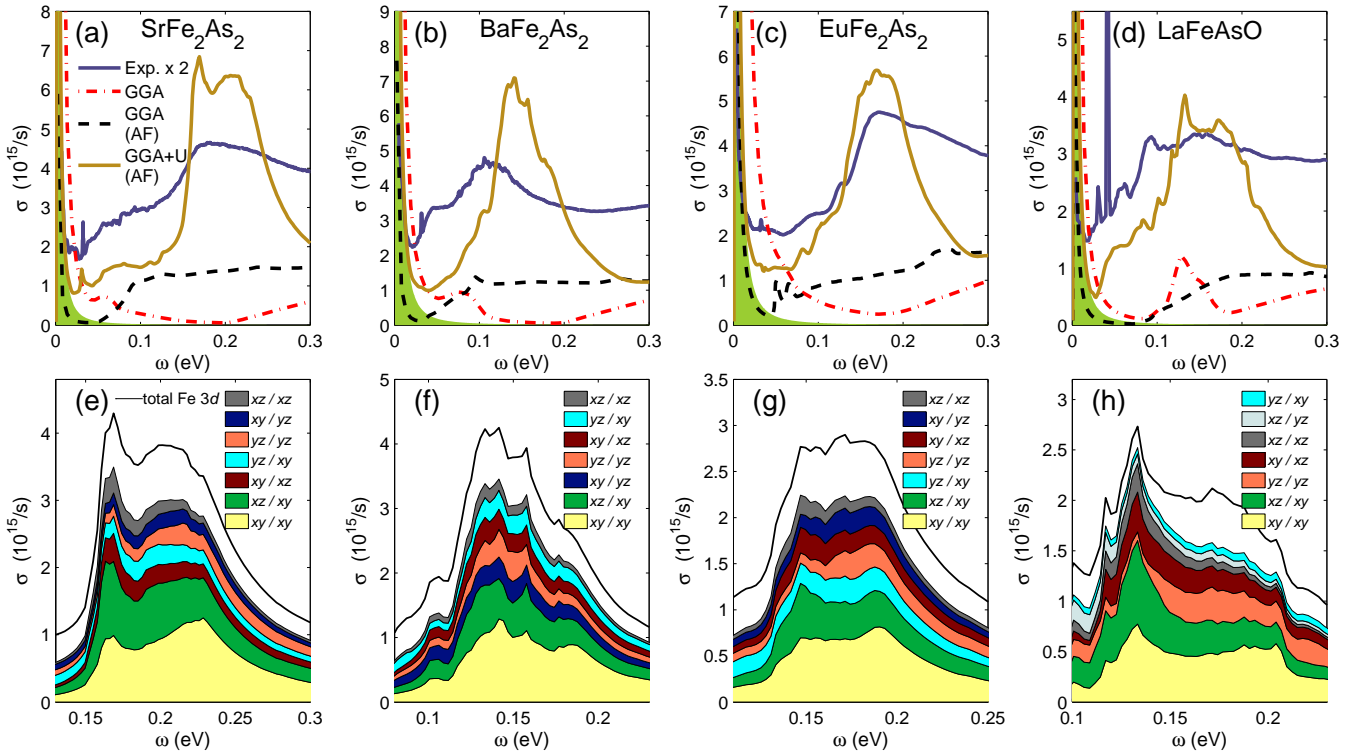


FIG. 2. (Color online) Real part of the optical conductivity of different iron pnictides in the SDW state, for $U_{\text{eff}} = -1.9$ eV: (a),(e) SrFe_2As_2 (experimental data taken from Ref. 5), (b),(f) BaFe_2As_2 (Ref. 5), (c),(g) EuFe_2As_2 (Ref. 31), and (d),(h) LaFeAsO (Ref. 11). No (empirical) Lorentz broadening has been applied; in order to facilitate the comparison with the damped/broadened experimental data, the experimental results have been rescaled by a factor of two. The orbital character contributions are sorted by their contribution to the total conductivity, integrated over the energy range shown in the respective plot, with the largest contribution at the bottom (for clarity, only the first seven contributions are displayed; smaller contributions have been omitted).

gap is $\Delta \approx 0.17$ eV. Almost over the whole energy range shown in the figure, the DOS is strongly distorted and shifted by the inclusion of the antiferromagnetic order compared to the non-spin-polarized GGA DOS. However, the strong suppression of the magnetic moments for $U_{\text{eff}} = -1.9$ eV renders the DOS almost equal to the GGA DOS again, except in the region around the Fermi energy. Thus, the optical properties can be expected to be close to the GGA case in the higher energy regions of the spectrum.

B. Optical conductivity

As for the in-plane optical conductivity of the iron pnictides in the SDW state, experimental investigations on single crystals^{5,11,31,58} consistently report a number of common features, although the exact location of the features depends on the material under investigation. These features are: metallic behaviour, *i.e.* the presence of a Drude-like conductivity at low frequencies ($\lesssim 100$ cm^{-1}), a sharp peak at the SDW gap frequency (≈ 1000 cm^{-1} – 1500 cm^{-1}), and a broad, less pronounced peak in the midinfrared region (≈ 5000 cm^{-1} – 6000 cm^{-1}) which

almost doesn't depend on temperature and is present also above T_{SDW} . The peaks are associated with a suppression of the spectral weight at lower energies (below ≈ 1000 cm^{-1} for the SDW peak, below ≈ 5000 cm^{-1} for the high-energy peak) which leads to a spectral weight transfer from lower to higher energies. Note that in the normal state, the tetragonal symmetry leaves only two independent components in the dielectric tensor and thus the conductivity is defined as $\sigma_{aa} = \sigma_{bb}$ for the Fe in-plane directions a and b , and σ_{cc} for the out-of-plane direction c perpendicular to a and b . In the SDW state, the stripe-like AF order introduces an anisotropy which lifts the degeneracy of the two in-plane components. However, no substantial anisotropy is found experimentally.

In Fig. 2 we present an overview of the in-plane optical conductivity in the low-frequency region as obtained by our calculations. Figs. 2 (a)–(d) show a comparison of the experimental results with the calculation methods introduced in the previous section; the GGA+U(AF) results exhibit the SDW peak as the most prominent feature, located at the SDW gap frequency. For all compounds, the SDW peak emerges at the experimentally determined frequency only for a suitable negative value of U_{eff} , and otherwise moves to higher frequencies (see

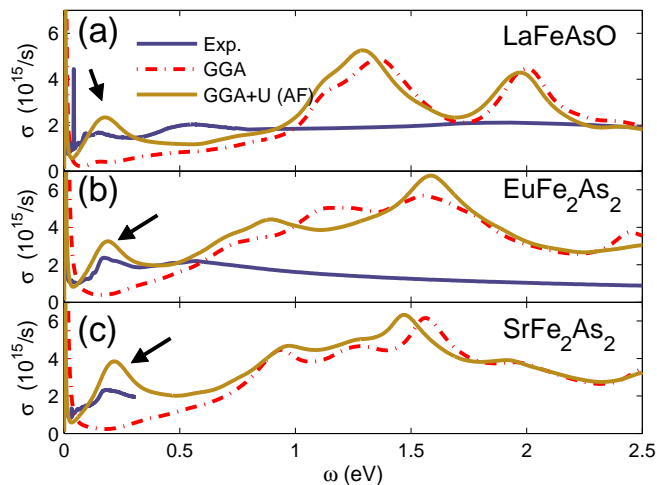


FIG. 3. (Color online) Optical conductivity in the higher energy region for (a) LaFeAsO, (b) BaFe₂As₂, and (c) SrFe₂As₂. Same experimental references and values for U_{eff} as in Fig. 2. The arrows indicate the position of the respective SDW peak.

Fig. 4 for SrFe₂As₂). The value $U_{\text{eff}} = -1.9$ eV was approximately determined by demanding a correct SDW peak position. Fig. 3 displays the optical conductivity for LaFeAsO, BaFe₂As₂, and SrFe₂As₂ over a larger energy range and includes some damping. As can be seen there, the GGA results without SDW order don't show any significant peak in the optical conductivity up to ≈ 1 eV. This can be readily read off from the density of states, where the GGA DOS is essentially depleted up to 1 eV above E_F . At higher energies, there is an obvious disagreement between the DFT results and the experimental data, for both GGA+U(AF) and GGA. Whereas we already mentioned the midinfrared peak around 0.6 eV, the experimental data basically doesn't show any structure above 1 eV. This could be described if quantum fluctuations are treated properly and consequently a frequency-dependent self-energy is involved. However, as the focus of this work is the analysis of the features induced by the antiferromagnetic ordering, we concentrate on the low energy features as indicated by the arrows.

As for the anisotropy due to the stripe-type SDW symmetry-breaking, we find that it is strongly present in the GGA(AF) calculation (*i.e.* for $U_{\text{eff}} = 0$) and for moderately negative values $U_{\text{eff}} \gtrsim -1.5$ eV, where σ_{bb} – the conductivity along the FM axis – shows a peak at significantly higher frequencies than σ_{aa} . In fact, this anisotropy can be mapped to the DOS in Fig. 1, where t_1 denotes the transition(s) which dominate the peak in σ_{bb} and t_2 the ones dominating σ_{aa} . As U_{eff} is decreased, the anisotropy is gradually suppressed and for the regime shown in Fig. 2, almost no anisotropy is present anymore in SrFe₂As₂, BaFe₂As₂ and EuFe₂As₂, in accordance with the experimental observations. This can be understood by the fact that while d_{xz} and d_{yz} are degenerate in the high temperature tetragonal phase, below

the SDW transition temperature, different band splittings and band shiftings are produced by different magnetization and occupation number on these two orbitals. Therefore, the excitations along x and y direction become inequivalent. As U_{eff} is decreased, the magnetization and consequently the symmetry-breaking between d_{xz} and d_{yz} orbitals are suppressed, leading to smaller differences between d_{xz} and d_{yz} orbitals and accordingly in the excitations along x and y direction. An anisotropy can still be seen in the weak double peak structure of LaFeAsO and SrFe₂As₂ in Figs. 2 (d) and (h), respectively (a) and (e) (the conductivity shown in the plots is given by $\sigma = (\sigma_{aa} + \sigma_{bb})/2$): e.g. in LaFeAsO, the d_{xy} contribution is of roughly equal size in both sub-peaks, whereas the d_{xz} contribution is mainly present in the first sub-peak and the d_{yz} contribution in the second one. Consequently, the second sub-peak is dominated by σ_{bb} , *i.e.* by the conductivity along the FM direction. We want to point out that also this sub-peak is directly related to the AF order as no peak is present in a purely ferromagnetic calculation (with the same absolute value of the magnetic moments).

The observed midinfrared peak at ≈ 0.6 eV, which is visible in Fig. 3 for LaFeAsO and BaFe₂As₂, respectively, is absent in all calculations, including the non-spin-polarized GGA calculations. This is in contrast to the experimental data and needs to be investigated further.

Surprisingly, the calculated optical spectrum of SrFe₂As₂ shows an experimentally observed low-frequency feature at 31 meV (see Fig. 2(a)) that has so far been attributed to phononic excitations: while there is no discussion in the respective experimental work Ref. 5 for SrFe₂As₂, for EuFe₂As₂ it is argued in Ref. 32 that the phononic mode – there at 32 meV – exhibits a coupling to the electronic background only for high temperatures while for low temperatures the Lorentz line shapes indicates a purely phononic, non-interacting excitation. However, our results show that this peak can also be obtained from the electronic band structure alone in SrFe₂As₂.

In Figs. 2 (e)–(h), the decomposition of the SDW peak into Fe 3d orbital characters of the initial and final states is shown. The orbital resolved optical conductivity reads

$$\sigma^{m_i, m_f}(\omega) = \frac{\hbar^2 e^2}{4\pi^2 m^2 \omega} \sum_{v, c} \int_{\mathbf{k}} A_{c, \mathbf{k}}^{m_f} |\langle c, \mathbf{k} | p | v, \mathbf{k} \rangle|^2 \times A_{v, \mathbf{k}}^{m_i} \delta(E_{c, \mathbf{k}} - E_{v, \mathbf{k}} - \hbar\omega), \quad (8)$$

where $A_{n, \mathbf{k}}^m$ formally denotes the relative weight of the Fe orbitals with magnetic quantum number m in the KS orbital $|n, \mathbf{k}\rangle$. Note that the momentum operators only couple states with different parity, reflected by the well known selection rule $\Delta l = l_f - l_i = \pm 1$ for dipolar transitions. Dipolar transitions among Fe 3d states are therefore forbidden in the atomic limit. For the iron pnictides, the states around the Fermi energy are Fe 3d dominated with some As 4p contribution. This hybridisation al-

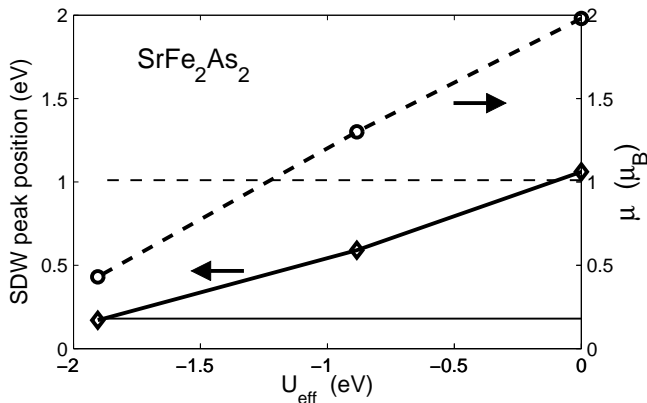


FIG. 4. Dependence of the SDW peak position in the optical conductivity and the magnetic moment on the value of U_{eff} for SrFe_2As_2 . The thin lines indicate experimental values: $\mu_{\text{exp}} = 1.01\mu_B$ ^{46,47}, $\text{SDW}_{\text{exp}} = 0.18 \text{ eV}$ ⁵

lows for transitions between initial and final states which are both Fe $3d$ dominated but owe their finite transition strength to Fe $3d \leftrightarrow$ As $4p$ transitions. This is taken into account in Eq. (8) where the full wavefunction $|n, \mathbf{k}\rangle$ is used for the calculation of the matrix element but the resulting dielectric function is projected on the Fe $3d$ subspace. This projection in particular omits the contribution from the interstitial region which has a considerable DOS in the considered energy range but cannot be assigned an orbital character. However, as can be seen from the comparison of the SDW peaks in Figs. 2 (a)–(d) – which show the total optical conductivity – to the close-up in (e)–(h) – which only show the Fe $3d$ contribution –, the Fe $3d$ part resembles very well the structure of the total conductivity. Therefore the contributions from the interstitial region as well as from the other atoms are neglected for the orbital character analysis.

In the iron pnictides, the Fermi surface is crossed by multiple bands. Consequently, also the optical properties have multiband nature and one can expect contributions from several orbital characters. This is confirmed by our calculations where we observe no overly dominating character component in any part of the spectrum. The SDW peak structure differs from the rest of the spectrum in that it mainly contains t_{2g} character components; all t_{2g} components are larger than any e_g component.

Finally, we analyze the low-energy Drude region of the spectrum as characterized by the plasma frequency. Since the SDW gap opening is only partial, the Drude peak is still present – expressed by a finite plasma frequency – both experimentally and in our calculations. The ratio of the kinetic energies which equals the ratio of the squares of the plasma frequencies, $K_{\text{exp}}/K_{\text{band}} = (\omega_p^{\text{exp}})^2/(\omega_p^{\text{band}})^2$, is commonly taken as a measure for the renormalization effect from the electronic correlations compared to band structure calculations. As given in Table I, the non-spin-polarized GGA value for, *e.g.*,

TABLE I. Optical parameters of the investigated compounds as obtained from the different calculation methods. $\omega_p^{a(b)}$ is the plasma frequency in $a(b)$ -direction.

Compound	Calc.	ω_p^a [eV]	ω_p^b [eV]	# bands at E_F	m [μ_B]
LaFeAsO	GGA	2.25	2.25	5	0
	GGA(AF)	0.87	0.82	2	1.98
	GGA+U(AF), $U_{\text{eff}} = -1.9\text{eV}$	1.74	1.17	2	0.29
BaFe ₂ As ₂	GGA	2.62	2.62	5	0
	GGA(AF)	0.62	0.65	2	1.98
	GGA+U(AF), $U_{\text{eff}} = -1.9\text{eV}$	1.66	1.53	3	0.30
SrFe ₂ As ₂	GGA	2.79	2.79	5	0
	GGA(AF)	0.64	0.64	2	1.98
	GGA+U(AF), $U_{\text{eff}} = -1.9\text{eV}$	1.50	1.27	2	0.43
EuFe ₂ As ₂	GGA	2.96	2.96	5	0
	GGA(AF)	0.84	0.99	2	1.76
	GGA+U(AF), $U_{\text{eff}} = -1.9\text{eV}$	1.95	2.04	3	0.34

SrFe_2As_2 is $\omega_p \approx 2.79 \text{ eV}$, whereas the experimental value in the normal state is $\omega_p \approx 1.7 \text{ eV}$ at 300 K,⁵ yielding $K_{\text{exp}}/K_{\text{band}} \approx 0.37$. In the SDW state, the experimental plasma frequency is strongly reduced due to the removal of itinerant carriers from the Fermi surface by the opening of the SDW gap, to $\omega_p \approx 0.59 \text{ eV}$ at 10 K.⁵ Likewise, in our calculations, the inclusion of the SDW order reduces the number of bands crossing the Fermi surface, which also significantly reduces the plasma frequencies. The renormalization due to the correlations still persists, though: with $K_{\text{exp}}/K_{\text{band}} \approx 0.15$ at $U_{\text{eff}} = -1.9 \text{ eV}$ it is even more pronounced in the SDW state.

In Table I as well as Fig. 4, one also notices that with our choices of U_{eff} in the GGA+U(AF) calculations, experimental SDW peak positions are well reproduced, while the calculated magnetic moments are all smaller than the corresponding experimental values, for example, the calculated magnetic moment for SrFe_2As_2 is $0.43\mu_B$ while it is $1.01\mu_B$ from neutron diffraction experiments^{46,47}. The discrepancy is due to the fact that the employed RPA scheme neglects correlation effects, like interactions between electrons and holes which may reduce the excitation energy and would therefore shift the SDW peak towards lower frequencies. In order to account for such a shift induced by correlation effects, a smaller value of the magnetic moment compared to the experimental one has to be used, which similarly shifts the SDW peak towards a lower position. For LaFeAsO, the discrepancy between the calculated magnetic moment, with which the experimentally observed SDW peak position is reproduced, and the experimental one is less pronounced, indicating less correlation strength in LaFeAsO than in

the other three compounds which is consistent with the DFT downfolding results of Ref. 48.

For all compounds except EuFe_2As_2 , the plasma frequencies and thus the dc conductivities exhibit a notable anisotropy between the a and b axis. Interestingly, the anisotropy develops differently in the 1111 compound and the 122 compounds where the 1111 compound always features a higher conductivity along the a direction. In contrast, $\sigma^b > \sigma^a$ in the 122 compounds for $U_{\text{eff}} = 0$ which is expected because of the larger lattice constant along the a axis and the orientation of the SDW vector along a . Unexpectedly, this no longer holds for negative U_{eff} where we find $\sigma^a > \sigma^b$ also for the 122 compounds. This is in agreement with recent experiments on underdoped BaFe_2As_2 where the magnetic domains were (partially) detwinned in a magnetic field in order to reveal the in-plane anisotropy in the resistivity.⁴⁹

IV. CONCLUSIONS

In summary we have demonstrated that DFT is capable to reproduce a number of features associated with the SDW state in the iron pnictides. However, this comes at the cost of a negative U_{eff} in the context of GGA+U calculations. The negative U may be understood as a way of

simulating a strong screening of the Coulomb interaction and a large electron-phonon coupling^{50–52,55–57}. Also it can be viewed as a route to mimic the effects of quantum fluctuations at the mean-field level and therefore as a driving force for suppressing the overestimated Fe magnetic moments obtained from GGA(AF). Concerning the size of the magnetic moments and thus the position of the SDW peak, the negative U_{eff} therefore needs to be interpreted as a fitting parameter. However, the agreement with the experimentally observed isotropy of the in-plane conductivity and the appearance of the low-frequency phononic-electronic excitation at exactly the right frequency indicate the reliability of the approach. Therefore, we conclude that the used LDA+U framework with negative U_{eff} mainly reduces the magnetic moment but doesn't distort the overall band structure too seriously. This suggests that this method is surprisingly well suited for the description of the SDW state in the iron pnictides.

Acknowledgements.- We would like to thank M. Dreschel, N. Barišić, N. Drichko, J. Fink and K. Foyevtsova for useful discussions. We gratefully acknowledge financial support from the Deutsche Forschungsgemeinschaft through the SPP 1458 program and from the Helmholtz Association through HA216/EMMI.

* ferber@itp.uni-frankfurt.de

- ¹ See review by K. Ishida, Y. Nakai, and H. Hosono, J. Phys. Soc. Jpn. **78**, 062001 (2009), and references therein.
- ² See review by J. W. Lynn and P. Dai, Physica C **469**, 469 (2009), and references therein.
- ³ Y. Kamihara, T. Watanabe, M. Hirano, and H. Hosono, J. Am. Chem. Soc. **130**, 3296 (2008).
- ⁴ M. S. Torikachvili, S. L. Bud'ko, N. Ni, and P. C. Canfield, Phys. Rev. Lett. **101**, 057006 (2008).
- ⁵ W. Z. Hu, J. Dong, G. Li, Z. Li, P. Zheng, G. F. Chen, J. L. Luo, and N. L. Wang, Phys. Rev. Lett. **101**, 257005 (2008).
- ⁶ D. Hsieh, Y. Xia, L. Wray, D. Qian, K. Gomes, A. Yazdani, G. F. Chen, J. L. Luo, N. L. Wang, and M. Z. Hasan (2008), arXiv:0812.2289.
- ⁷ M. Yi, D. H. Lu, J. G. Analytis, J.-H. Chu, S.-K. Mo, R.-H. He, M. Hashimoto, R. G. Moore, I. I. Mazin, D. J. Singh, et al., Phys. Rev. B **80**, 174510 (2009).
- ⁸ J. Fink, S. Thirupathaiah, R. Ovsyannikov, H. A. Dürr, R. Follath, Y. Huang, S. de Jong, M. S. Golden, Y.-Z. Zhang, H. O. Jeschke, et al., Phys. Rev. B **79**, 155118 (2009).
- ⁹ S. A. J. Kimber, A. Kreyssig, Y.-Z. Zhang, H. O. Jeschke, R. Valentí, F. Yokaichiya, E. Colombier, J. Yan, T. C. Hansen, T. Chatterji, et al., Nature Mater. **8**, 471 (2009).
- ¹⁰ S. Thirupathaiah, S. de Jong, R. Ovsyannikov, H. A. Dürr, A. Varykhalov, R. Follath, Y. Huang, R. Huisman, M. S. Golden, Y.-Z. Zhang, et al., Phys. Rev. B **81**, 104512 (2010).
- ¹¹ Z. G. Chen, R. H. Yuan, T. Dong, and N. L. Wang, Phys. Rev. B **81**, 100502(R) (2010).

- ¹² I. I. Mazin, D. J. Singh, M. D. Johannes, and M. H. Du, Phys. Rev. Lett. **101**, 057003 (2008).
- ¹³ J. Dong, H. J. Zhang, G. Xu, Z. Li, G. Li, W. Z. Hu, D. Wu, G. F. Chen, X. Dai, J. L. Luo, et al., Europhys. Lett. **83**, 27006 (2008).
- ¹⁴ V. Cvetkovic and Z. Tesanovic, Europhys. Lett. **85**, 37002 (2009).
- ¹⁵ I. Opahle, H. C. Kandpal, Y. Zhang, C. Gros, and R. Valentí, Phys. Rev. B **79**, 024509 (2009).
- ¹⁶ Y.-Z. Zhang, H. C. Kandpal, I. Opahle, H. O. Jeschke, and R. Valentí, Phys. Rev. B **80**, 094530 (2009).
- ¹⁷ A. N. Yaresko, G.-Q. Liu, V. N. Antonov, and O. K. Andersen, Phys. Rev. B **79**, 144421 (2009).
- ¹⁸ Y.-Z. Zhang, I. Opahle, H. O. Jeschke, and R. Valentí, Phys. Rev. B **81**, 094505 (2010).
- ¹⁹ H. Lee, Y.-Z. Zhang, H. O. Jeschke, and R. Valentí (2009), arXiv:0912.4024.
- ²⁰ M. Aichhorn, L. Pourovskii, V. Vildosola, M. Ferrero, O. Parcollet, T. Miyake, A. Georges, and S. Biermann, Phys. Rev. B **80**, 085101 (2009).
- ²¹ S. L. Skornyakov, A. V. Efremov, N. A. Skorikov, M. A. Korotin, Y. A. Izyumov, V. I. Anisimov, A. V. Kozhevnikov, and D. Vollhardt, Phys. Rev. B **80**, 092501 (2009).
- ²² L. X. Yang, Y. Zhang, H. W. Ou, J. F. Zhao, D. W. Shen, B. Zhou, J. Wei, F. Chen, M. Xu, C. He, et al., Phys. Rev. Lett. **102**, 107002 (2009).
- ²³ Q. Si and E. Abrahams, Phys. Rev. Lett. **101**, 076401 (2008).
- ²⁴ K. Haule, J. H. Shim, and G. Kotliar, Phys. Rev. Lett. **100**, 226402 (2008).

- ²⁵ T. Yildirim, Phys. Rev. Lett. **101**, 057010 (2008).
- ²⁶ M. J. Han, Q. Yin, W. E. Pickett, and S. Y. Savrasov, Phys. Rev. Lett. **102**, 107003 (2009).
- ²⁷ F. Ma, W. Ji, J. Hu, Z.-Y. Lu, and T. Xiang, Phys. Rev. Lett. **102**, 177003 (2009).
- ²⁸ M. M. Qazilbash, J. J. Hamlin, R. E. Baumbach, L. Zhang, D. J. Singh, M. B. Maple, and D. N. Basov, Nature Phys. **5**, 647 (2009).
- ²⁹ S.-L. Drechsler, M. Grobosch, K. Koepf, G. Behr, A. Köhler, J. Werner, A. Kondrat, N. Leps, C. Hess, R. Klingeler, et al., Phys. Rev. Lett. **101**, 257004 (2008).
- ³⁰ M. Nakajima, S. Ishida, K. Kihou, Y. Tomioka, T. Ito, Y. Yoshida, C. H. Lee, H. Kito, A. Iyo, H. Eisaki, et al., Phys. Rev. B **81**, 104528 (2010).
- ³¹ D. Wu, N. Barišić, P. Kallina, A. Faridian, B. Gorshunov, N. Drichko, L. J. Li, X. Lin, G. H. Cao, Z. A. Xu, et al., Phys. Rev. B **81**, 100512(R) (2010).
- ³² D. Wu, N. Barišić, N. Drichko, S. Kaiser, A. Faridian, M. Dressel, S. Jiang, Z. Ren, L. J. Li, G. H. Cao, et al., Phys. Rev. B **79**, 155103 (2009).
- ³³ B. Gorshunov, D. Wu, A. A. Voronkov, P. Kallina, K. Iida, S. Haindl, F. Kurth, L. Schultz, B. Holzapfel, and M. Dressel, Phys. Rev. B **81**, 060509(R) (2010).
- ³⁴ M. S. Laad, L. Craco, S. Leoni, and H. Rosner, Phys. Rev. B **79**, 024515 (2009).
- ³⁵ P. Blaha, K. Schwarz, G. K. H. Madsen, D. Kvasnicka, and J. Luitz, *WIEN2k, An Augmented Plane Wave + Local Orbitals Program for Calculating Crystal Properties* (Techn. Universität Wien, Austria, 2001).
- ³⁶ J. P. Perdew, K. Burke, and M. Ernzerhof, Phys. Rev. Lett. **77**, 3865 (1996).
- ³⁷ T. Nomura, S. W. Kim, Y. Kamihara, M. Hirano, P. V. Sushko, K. Kato, M. Takata, A. L. Shluger, and H. Hosono, Supercond. Sci. Tech. **21**, 125028 (2008).
- ³⁸ Q. Huang, Y. Qiu, W. Bao, M. A. Green, J. W. Lynn, Y. C. Gasparovic, T. Wu, G. Wu, and X. H. Chen, Phys. Rev. Lett. **101**, 257003 (2008).
- ³⁹ P. L. Alireza, Y. T. C. Ko, J. Gillett, C. M. Petrone, J. M. Cole, G. G. Lonzarich, and S. E. Sebastian, J. Phys.: Condens. Matter **21**, 012208 (2009).
- ⁴⁰ M. Tegel, M. Rotter, V. Weiß, F. M. Schappacher, R. Pöttgen, and D. Johrendt, J. Phys.: Condens. Matter **20**, 452201 (2008).
- ⁴¹ C. Ambrosch-Draxl and J. O. Sofo, Comp. Phys. Commun. **175**, 1 (2006).
- ⁴² V. I. Anisimov, I. V. Solovyev, M. A. Korotin, M. T. Czyżyk, and G. A. Sawatzky, Phys. Rev. B **48**, 16929 (1993).
- ⁴³ C. de la Cruz, Q. Huang, J. W. Lynn, J. Li, W. R. II, J. L. Zarestky, H. A. Mook, G. F. Chen, J. L. Luo, N. L. Wang, et al., Nature (London) **453**, 899 (2008).
- ⁴⁴ N. Qureshi, Y. Drees, J. Werner, S. Wurmehl, C. Hess, R. Klingeler, B. Büchner, M. T. Fernandez-Diaz, and M. Braden (2010), arXiv:1002.4326.
- ⁴⁵ H. Nakamura, N. Hayashi, N. Nakai, M. Okumura, and M. Machida, Physica C **469**, 908 (2009).
- ⁴⁶ K. Kaneko, A. Hoser, N. Caroca-Canales, A. Jesche, C. Krellner, O. Stockert, and C. Geibel, Phys. Rev. B **78**, 212502 (2008).
- ⁴⁷ A. Jesche, N. Caroca-Canales, H. Rosner, H. Borrmann, A. Ormeci, D. Kasinathan, H. H. Klauss, H. Luetkens, R. Khasanov, A. Amato, et al., Phys. Rev. B **78**, 180504(R) (2008).
- ⁴⁸ T. Miyake, K. Nakamura, R. Arita, and M. Imada, J. Phys. Soc. Jpn. **79**, 044705 (2010).
- ⁴⁹ J.-H. Chu, J. G. Analytis, D. Press, K. D. Greve, T. D. Ladd, Y. Yamamoto, and I. R. Fisher (2009), arXiv:0911.3878.
- ⁵⁰ R. H. Liu, T. Wu, G. Wu, H. Chen, X. F. Wang, Y. L. Xie, J. J. Ying, Y. J. Yan, Q. J. Li, B. C. Shi, et al., Nature (London) **459**, 64 (2009).
- ⁵¹ P. M. Shirage, K. Kihou, K. Miyazawa, C.-H. Lee, H. Kito, H. Eisaki, T. Yanagisawa, Y. Tanaka, and A. Iyo, Phys. Rev. Lett. **103**, 257003 (2009).
- ⁵² M. Rahnbeck, G. L. Sun, D. L. Sun, C. T. Lin, B. Keimer, and C. Ulrich, Phys. Rev. B **80**, 064509 (2009).
- ⁵³ E. R. Ylvisaker, W. E. Pickett, and K. Koepf, Phys. Rev. B **79**, 035103 (2009).
- ⁵⁴ S. L. Dudarev, G. A. Botton, S. Y. Savrasov, C. J. Humphreys, and A. P. Sutton, Phys. Rev. B **57**, 1505 (1998).
- ⁵⁵ K.-Y. Choi, P. Lemmens, I. Eremin, G. Zwicknagl, H. Berger, G. L. Sun, D. L. Sun, and C. T. Lin, J. Phys.: Condens. Matter **22**, 115802 (2010).
- ⁵⁶ A. A. Kordyuk, V. B. Zabolotnyy, D. V. Evtushinsky, T. K. Kim, I. V. Morozov, M. L. Kulić, R. Follath, G. Behr, B. Büchner, and S. V. Borisenko (2010), arXiv:1002.3149.
- ⁵⁷ L. Boeri, M. Calandra, I. I. Mazin, O. V. Dolgov, and F. Mauri (2010), arXiv:1004.1943.
- ⁵⁸ A. Lucarelli, A. Dusza, F. Pfüner, P. Lerch, J. G. Analytis, J. H. Chu, I. R. Fisher, and L. Degiorgi (2010), arXiv:1004.3022.
- ⁵⁹ Phononic excitations are not considered in this work